A study of the predissociation of NaK molecules in the 6 $^1\Sigma^+$ state by optical–optical double resonance spectroscopy

Z. J. Jabbour[a)] and J. Huennekens

Department of Physics, Lehigh University, Bethlehem, Pennsylvania 18015

Predissociation of a high-lying $^1\Sigma^+$ state of NaK is studied using the optical–optical double resonance technique. A single-mode ring dye laser is set to a particular $2(A)^1\Sigma^+(v',J')\leftarrow 1(X)^1\Sigma^+(v'',J'')$ transition. Another single-mode laser (Ti–sapphire) is then used to excite the molecule from the $2(A)^1\Sigma^+(v',J')$ level, to rovibrational levels of a higher predissociating electronic state, which we identify as $6\,^1\Sigma^+$. The predissociation is monitored by the atomic potassium emission on the $3\,^2D_{3/2}\rightarrow 4\,^2P_{1/2}$ transition at 1.17 μm, while bound state radiative processes are monitored by total violet fluorescence from the upper state to the various rovibrational levels of the ground $1(X)^1\Sigma^+$ state. By scanning the Ti–sapphire laser, different rovibrational levels of the $6\,^1\Sigma^+$ state can be excited. The vibrational levels probed range from $v=13$ to 20 with rotational states ranging from 9 to 99. The bound state energy level positions are measured from the center frequencies of lines recorded with the Ti–sapphire laser excitation scans. The $6\,^1\Sigma^+$ state is then described by the following molecular constants which are calculated from the experimental values of the level energies: $T_e=25\,560.373$ cm^{-1}, $\omega_e=89.179\,26$ cm^{-1}, $\omega_e x_e=0.730\,691$ cm^{-1}, $B_e=0.067\,327\,0$ cm^{-1}, $\alpha_e=0.000\,675\,35$ cm^{-1}, $D_e=-3.298\,31\times 10^{-8}$ cm^{-1}, $\beta_{el}=1.518\,17\times 10^{-8}$ cm^{-1}. The potential well depth is $D_e=4416.0$ cm^{-1}, if we assume the most likely asymptotic limit of Na($3\,^2S_{1/2}$)+K($5\,^2P_{1/2}$). The equilibrium separation is $R_e=4.158$ Å. We also report measured and calculated intensities (Franck–Condon factors) for the $6\,^1\Sigma^+\rightarrow 1(X)^1\Sigma^+$ violet band. The absolute predissociation rates of $6\,^1\Sigma^+$ levels are directly measured from the linewidths recorded on the Ti–sapphire laser excitation scans. We measure predissociation rates ranging up to 9.4×10^9 s^{-1}. The dependence of the absolute predissociation rates on rovibrational quantum numbers is studied with an attempt to predict the shape of the repulsive potential curve causing the predissociation, its crossing point with the bound state, and the type of perturbative interaction leading to the predissociation. The state causing the predissociation is determined from correlation diagrams to be the continuum of either the $3\,^3\Pi$, the $3\,^1\Pi$, or the $5\,^3\Sigma^+$ state with Na($3S$)+K($3D$) dissociation limit. We measure the collisional broadening rate coefficients of some $6\,^1\Sigma^+\leftarrow 2(A)^1\Sigma^+$ lines due to both argon and potassium perturbers, and obtain the average values, $k_{br}^{\mathrm{Ar}}=(1.1\pm0.2)\times 10^{-8}$ cm^3 s^{-1} and $k_{br}^{\mathrm{K}}=(1.1\pm0.6)\times 10^{-8}$ cm^3 s^{-1}. Velocity-changing collisions and collisional excitation transfer between individual rotational levels of the $2(A)^1\Sigma^+$ state are also investigated. © *1997 American Institute of Physics.* [S0021-9606(97)00628-4]

I. INTRODUCTION

The predissociation of alkali diatomic molecules has been a subject of interest for many years (see Refs. 1–12). Predissociation can be used as a means for probing repulsive states of a molecule and as a mechanism for producing excited or ground state atoms that are otherwise not present in the vapor. Our current interest in the predissociation of NaK molecules stems from earlier work involving the generation of coherent infrared emissions. Previous work in our lab,[13] involving high intensity pulsed dye lasers, showed that when a mixed sodium–potassium vapor is excited with two red laser photons in the range 720–750 nm, a coherent emission at 1.17 μm appears which corresponds to the K($3\,^2D_{3/2}$)$\rightarrow$K($4\,^2P_{1/2}$) atomic transition. Further studies

(see Ref. 13 for details) led us to believe that this coherent 1.17 μm emission results from a predissociation process involving the NaK molecule. The present article discusses our investigation of that predissociation process using high-resolution single-mode cw ring lasers, which provides detailed information on the predissociation process and the molecular potentials involved.

Stevens *et al.*[14] have calculated all NaK potentials up to the Na($3S$)+K($3D$) limit and Δ states corresponding to the Na($3D$)+K($4S$) and Na($4P$)+K($4P$) limits using full-valence configuration interaction computations with effective core potentials. Very recently, Magnier and Millié[15] used pseudopotential methods to calculate potentials up to the Na($3P$)+K($4P$) dissociation limit. On the experimental side, most previous spectroscopic studies of the NaK molecule have involved low lying states correlating to the ground state and first excited states in the separated atom

---

[a)]Present address: Automated Production Technology Division, Sound A147, NIST, Gaithersburg, Maryland 20899.
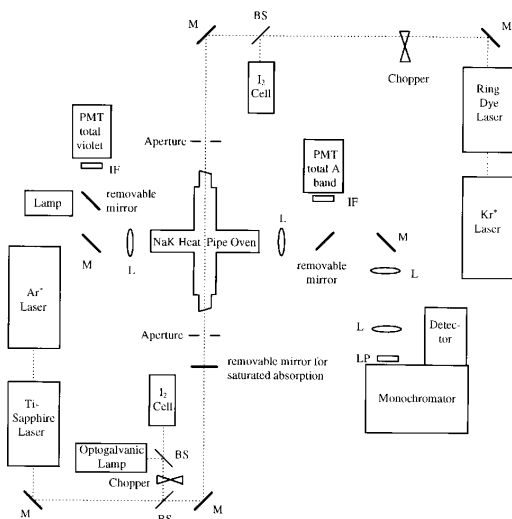
FIG. 1. Experimental setup. L, M, and BS represent lens, mirror, and beam-splitter, respectively, while LP, IF, and PMT refer to long pass filter, inter-ference filter, and photomultiplier tube, respectively.
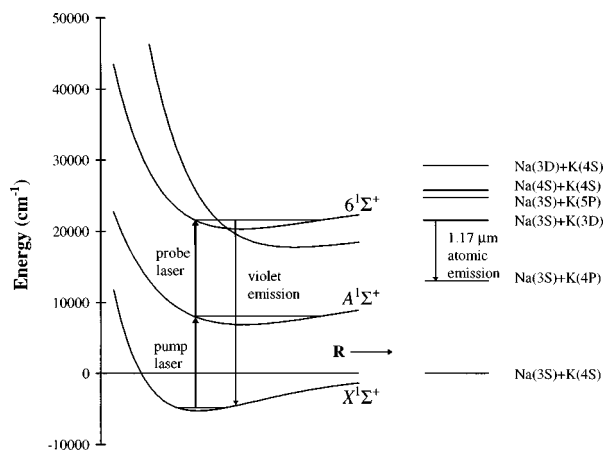

FIG. 2. Schematic energy level diagram of NaK showing the states of in-terest in the present work. Thick solid arrows represent the two-step pump-ing sequence $6\,^1\Sigma^+(v,J)\leftarrow 2(A)^1\Sigma^+(v',J')\leftarrow 1(X)^1\Sigma^+(v'',J'')$. Thin solid arrows represent the $6\,^1\Sigma^+(v,J)\rightarrow 1(X)^1\Sigma^+(v'',J\pm 1)$ violet molecu-lar fluorescence and the 1.17 μm K($3\,^2D_{3/2}$)$\rightarrow$K($4\,^2P_{1/2}$) atomic fluores-cence emissions which were monitored in this experiment.

limit. Experiments by Kasahara *et al.*[16] probed Rydberg states of NaK using the optical–optical double resonance spectroscopy technique. Recently, Berg *et al.* carried out femtosecond wave packet dynamics measurements of the $2(A)^1\Sigma^+$ state using the $E\,^1\Sigma^+\leftarrow 2(A)^1\Sigma^+$ probe transition in the wavelength range 755–832 nm,[17] and Hansson has studied the $E\,^1\Sigma^+$ state by one-color, two-photon excitation.[18] However, in general, the range of energies be-tween the low lying states and the Rydberg states has not been systematically investigated.

The present paper discusses the experimental observa-tion of the NaK violet band $[6\,^1\Sigma^+\rightarrow 1(X)^1\Sigma^+]$ and associ-ated Franck–Condon factors, the determination of the mo-lecular constants of the upper bound state, the investigation of the predissociation of that state to produce excited potas-sium atoms, the determination of the level by level predisso-ciation rates, the identification of both the bound and repul-sive states involved in the predissociation process including their dissociation limits, the collisional broadening of the bound-bound rovibrational molecular lines, and finally the J-changing and velocity-changing collisions involving NaK molecules in the $2(A)^1\Sigma^+$ state.

II. EXPERIMENT

The experimental setup is shown in Fig. 1. The sodium–potassium mixture is contained in a crossed heat-pipe oven using argon as a buffer gas. Two single-mode ring lasers (dye and Ti–sapphire—Coherent models 699-29 and 899-29) are used to study the two-step predissociation process. The ring dye laser is fixed in frequency to pump a specific (v',J') level of the NaK $2(A)^1\Sigma^+$ state from a level $(v'',J'\pm 1)$ of the $1(X)^1\Sigma^+$ ground state (see Fig. 2). The Ti–sapphire laser is then scanned across different rovibra-tional transitions coupling the $2(A)^1\Sigma^+$ state to a higher predissociating state that we later identify as $6\,^1\Sigma^+$. The two laser beams counterpropagate through the heat-pipe oven,

while fluorescence is detected at right angles to the laser propagation direction. Atomic fluorescence, corresponding to the potassium $3\,^2D_{3/2}\rightarrow 4\,^2P_{1/2}$ transition at 1.17 μm, is de-tected using a monochromator-Ge detector system. Free-standing photomultipliers with different interference filters are used for total molecular fluorescence detection. The total violet emissions consist of allowed transitions from a par-ticular $6\,^1\Sigma^+(v,J)$ level pumped through the two-step pro-cess, to all possible $(v'',J\pm 1)$ levels of the $1(X)^1\Sigma^+$ state. The total A band fluorescence includes all allowed transi-tions from the $2(A)^1\Sigma^+(v',J')$ level labeled with the ring dye laser to all possible $(v'',J'\pm 1)$ levels of the $1(X)^1\Sigma^+$ state. We use a removable mirror to detect the total A band fluorescence with a free-standing PMT on one side of the heat-pipe. When the mirror is removed and the Ge detector replaced by another PMT, resolved violet or A band fluores-cence transmitted through the monochromator can be moni-tored. On the other side of the heat-pipe, we monitor the total violet fluorescence. A removable mirror in the violet fluores-cence path allows light from a white light source to be trans-mitted through the heat-pipe, to the monochromator, for alignment purposes and to monitor atomic densities by ab-sorption.

The ring dye laser beam is chopped, while lock-in detec-tion techniques are used to detect fluorescence at the modu-lation frequency. This state-labeling technique ensures that all detected signals are produced by molecules that are pumped on the first step to the particular $2(A)^1\Sigma^+(v',J')$ level labeled by the ring dye laser. Doppler-free saturated absorption is used to find the line center of the $2(A)^1\Sigma^+(v',J')\leftarrow 1(X)^1\Sigma^+(v'',J'')$ transition. For this pur-pose, a removable mirror is used to retroreflect the ring dye laser beam upon itself. Laser-induced fluorescence from an iodine cell and the optogalvanic effect in a barium hollow cathode lamp are used to calibrate the laser wavemeters.

III. RESULTS AND DISCUSSION

A. Identification of the predissociating bound state

In this experiment, the second step laser (Ti–sapphire) can excite molecules from the $2(A)\,^1\Sigma^+$ state to a higher lying $^1\Pi$ or $^1\Sigma^+$ state according to the selection rules for electronic transitions; $\Delta\Lambda=0$, ± 1 and $\Delta S=0$. For $\Delta\Lambda=0$ ($^1\Sigma^+\leftarrow\,^1\Sigma^+$ transitions), the rotational quantum number J obeys the dipole selection rule $\Delta J=\pm 1$. For $^1\Pi\leftarrow\,^1\Sigma^+$ ($\Delta\Lambda=\pm 1$) transitions, the corresponding selection rule is $\Delta J=0$, ± 1.[19] Since the excitation spectra recorded by scanning the single-mode Ti–sapphire laser across different transitions coupling the labeled $2(A)\,^1\Sigma^+(v',J')$ level to various levels of the predissociating bound state exhibit a doublet structure, we can identify the predissociating bound state as having $^1\Sigma^+$ character.

We assign the dissociation (separated atom) limit of the predissociating $^1\Sigma^+$ state to $\text{Na}(3S)+\text{K}(5P)$ which is the next higher asymptotic limit above the $\text{Na}(3S)+\text{K}(3D)$ predissociation limit (see Fig. 2). This choice is not the only one possible, but it yields a reasonable well depth of 4416.0 cm^{-1}. Other possible asymptotes such as $\text{Na}(4S)+\text{K}(4S)$ and $\text{Na}(3D)+\text{K}(4S)$ yield well depths of 5454.4 and 8887.4 cm^{-1}, respectively.[20] Only the $\text{Na}(4S)+\text{K}(4S)$ asymptote is a reasonable alternative to $\text{Na}(3S)+\text{K}(5P)$. However, comparison with the recent theoretical potentials of Magnier and Millié[15] indicates that the correct limit is $\text{Na}(3S)+\text{K}(5P)$, and thus we identify the predissociating bound state as $6\,^1\Sigma^+$.

Absolute rotational numbering of intermediate $2(A)\,^1\Sigma^+(v',J')$ state levels is easily determined since these levels can be pumped from either of the two ground state levels $1(X)\,^1\Sigma^+(v'',J'\pm 1)$. Once a particular $2(A)\,^1\Sigma^+(v',J')\leftarrow 1(X)\,^1\Sigma^+(v'',J'\pm 1)$ transition is found and a preliminary assignment of J' is made, the laser frequency is shifted by $\Delta\nu=\{E[1(X)\,^1\Sigma^+(v',J'+1)]-E[1(X)\,^1\Sigma^+(v',J'-1)]\}/h$, calculated using the ground state constants of Ref. 21. If the assignment is correct, the same resolved A band fluorescence spectrum will be obtained. The absolute rotational numbering of $6\,^1\Sigma^+(v,J)$ levels can be determined since only the levels $6\,^1\Sigma^+(v,J'\pm 1)$ can be excited from $2(A)\,^1\Sigma^+(v',J')$. The absolute vibrational numbering of the $6\,^1\Sigma^+(v,J)$ levels is determined by comparison of measured and calculated Franck–Condon factors (see Sec. III C).

B. NaK $6\,^1\Sigma^+$ state molecular constants

The molecular energy levels can be described by a standard expansion in powers of the vibrational and rotational quantum numbers[19]

$$E(v,J)=T_e+G_v+F_v(J), \tag{1}$$

where T_e is the energy of the bottom of the potential well relative to the bottom of the ground state well, $G_v=\omega_e(v+1/2)-\omega_e x_e(v+1/2)^2+\omega_e y_e(v+1/2)^3+\cdots$ is the vibrational energy, and $F_v(J)=B_v J(J+1)-D_v J^2(J+1)^2+\cdots$

TABLE I. The molecular constants of the $6\,^1\Sigma^+$ state obtained in this work along with the theoretical constants of Ref. 15. Note that the well depth D_e should not be confused with the centrifugal distortion constant D_e. All values are given in cm^{-1} except for the equilibrium internuclear separation R_e which is in Å.

	Experiment (this work)	Theory (Ref. 15)
R_e	4.158	4.21
D_e	4416.0	4492
T_e	25 560.373±0.568	25445
ω_e	89.179 26±0.063 75	84.90
$\omega_e x_e$	0.730 691±0.001 769	
B_e	0.067 327 0±0.000 214 0	
α_e	$(6.753\ 5\pm0.116\ 8)\times10^{-4}$	
D_e	$(-3.298\ 31\pm1.775\ 57)\times10^{-8}$	
β_{e1}	$(1.518\ 17\pm0.098\ 98)\times10^{-8}$	

with $B_v=B_e-\alpha_e(v+1/2)+\gamma_{e1}(v+1/2)^2+\cdots$ and $D_v=D_e+\beta_{e1}(v+1/2)+\beta_{e2}(v+1/2)^2+\cdots$ defines the rotational energy.

The measured energy difference between the two vibrational levels $6\,^1\Sigma^+(v,J+1)$ and $6\,^1\Sigma^+(v,J-1)$ which can be excited from the same $2(A)\,^1\Sigma^+(v,J)$ level, is approximately given by[19]

$$\Delta_2 F_v(J)=F_v(J+1)-F_v(J-1)$$
$$\approx 4B_v(J+1/2)-8D_v(J+1/2)^3, \tag{2}$$

where the neglected terms introduce an error of only 0.003% in our B_v values.

We fit our measured values of $\Delta_2 F_v(J)/(J+1/2)$ as a function of $(J+1/2)^2$ to yield values of B_v and D_v. Fitting B_v and D_v as functions of $(v+1/2)$ then yields values for the constants B_e, α_e, D_e, and β_{e1}, where we assume that the lowest observed $6\,^1\Sigma^+$ vibrational level corresponds to $v=13$ (this assumption will be justified below). Finally, we fit the rotationless energies of each vibrational level, obtained by subtracting $F_v(J)$ from the measured level energies, as a function of $(v+1/2)$ to yield the constants T_e, ω_e, and $\omega_e x_e$.[19] The various $6\,^1\Sigma^+$ state molecular constants obtained in this work are listed in Table I, where they are compared to the theoretical constants of Ref. 15. Error bars in the table represent statistical errors only. The use of additional fitting parameters was considered to be unwarranted since our data cover only a limited range of vibrational levels.

The well depth of the $6\,^1\Sigma^+$ state is calculated from the measured T_e value (25 560.373 cm^{-1}), the well depth of the ground state ($D_e''=5274.9$ cm^{-1}, not to be confused with the centrifugal distortion constant D_e),[21] and the energy corresponding to the asymptotic limit $\{\Delta E = E[\text{Na}(3S_{1/2}) + \text{K}(5P_{1/2})] - E[\text{Na}(3S_{1/2}) + \text{K}(4S_{1/2})]=24\ 701.44$ cm$^{-1}\}$,[20] $D_e=\Delta E+D_e''-T_e=4416.0$ cm^{-1}. In a separate PAPS document,[22] we list the experimental $6\,^1\Sigma^+(v,J)$ level energies and compare them with those calculated using the constants in Table I. We note that the experimental energies of the $6\,^1\Sigma^+(v,J)\leftarrow 2(A)\,^1\Sigma^+(v',J')$ transitions are much more accurate than the $6\,^1\Sigma^+$ level energies calculated from the constants. For the 99 rovibrational levels observed

with $J < 69$, the rms deviation between the experimental energies and those calculated from the fitted constants is 0.15 cm^{-1}, while larger discrepancies are found for the 36 observed levels with $J \geqslant 69$. Much better agreement could be obtained by using a larger number of fitting constants. However, due to experimental constraints, we were only able to study vibrational levels in the range $v = 13$–20 in this work. Thus the extrapolation to the bottom of the potential well is questionable, and the use of additional fitting constants is likely to increase the errors in the extrapolation. Because of the long extrapolation, significant errors probably exist in the fitted constants (especially T_e and ω_e). Such errors are evident in the comparison of the experimental and theoretical Franck–Condon factors (see Sec. III C). Therefore, the physical significance of these rotational and vibrational constants must be taken with a grain of salt.

C. Franck–Condon factors of the NaK violet band: $6\,^1\Sigma^+ \rightarrow 1(X)^1\Sigma^+$

In the analysis described above, we assumed that the lowest observed vibrational level of the $6\,^1\Sigma^+$ state (designated as v_i) is given by $v_i = 13$. The procedure leading to this assumption is described below.

When the polynomial fits are carried out as outlined above, a value for v_i must be assumed in order to assign absolute vibrational quantum numbers and to carry out the calculations. Since v_i is not known initially, we assume a particular value, carry out the fits and find the molecular constants associated with our assignment. For each v_i assignment, we compute the RKR (Refs. 23–25) potential curve associated with the corresponding molecular constants derived from the experimental data.[26] From the RKR curves, we then calculate the Franck–Condon factors (FCF's), $|\int \psi_{v,J}\psi_{v'',J''}dR|^2$, for the violet molecular fluorescence transitions from one of the $6\,^1\Sigma^+(v,J)$ levels to various $1(X)^1\Sigma^+(v'',J\pm1)$ levels.[27] Here $\psi_{v,J}(R)$ and $\psi_{v'',J''}(R)$ are the upper and lower state vibrational wave functions. In the latter calculations, the $1(X)^1\Sigma^+$ state potential of Ross et al.[21] is used. The FCF's corresponding to each curve are then compared with the experimental relative intensities (divided by ν^4) since the latter are proportional to the former [assuming that the electronic transition dipole moment, $D_e(R)$, does not vary appreciably with R],[19,28]

$$I_{fl}(v,J \rightarrow v'',J'') = \frac{64\pi^4}{3}\,N_{v,J}\,\frac{S_{JJ''}}{2J+1}\,\frac{\nu^4}{c^3}\,[D_e(R)]^2$$

$$\times \left| \int \psi_{v,J}\psi_{v'',J''}dR \right|^2. \tag{3}$$

Here, $N_{v,J}$ is the number of molecules in the upper level, and $S_{JJ''}$ is the Hönl–London factor.[19] We assign the absolute vibrational numbering according to the best agreement of the calculated FCF's with the experimental data. The FCF's are very sensitive to the wave functions (and therefore to the potential curves). From this comparison, it appears that the lowest observed vibrational level in this case is most likely $v_i = 13$.
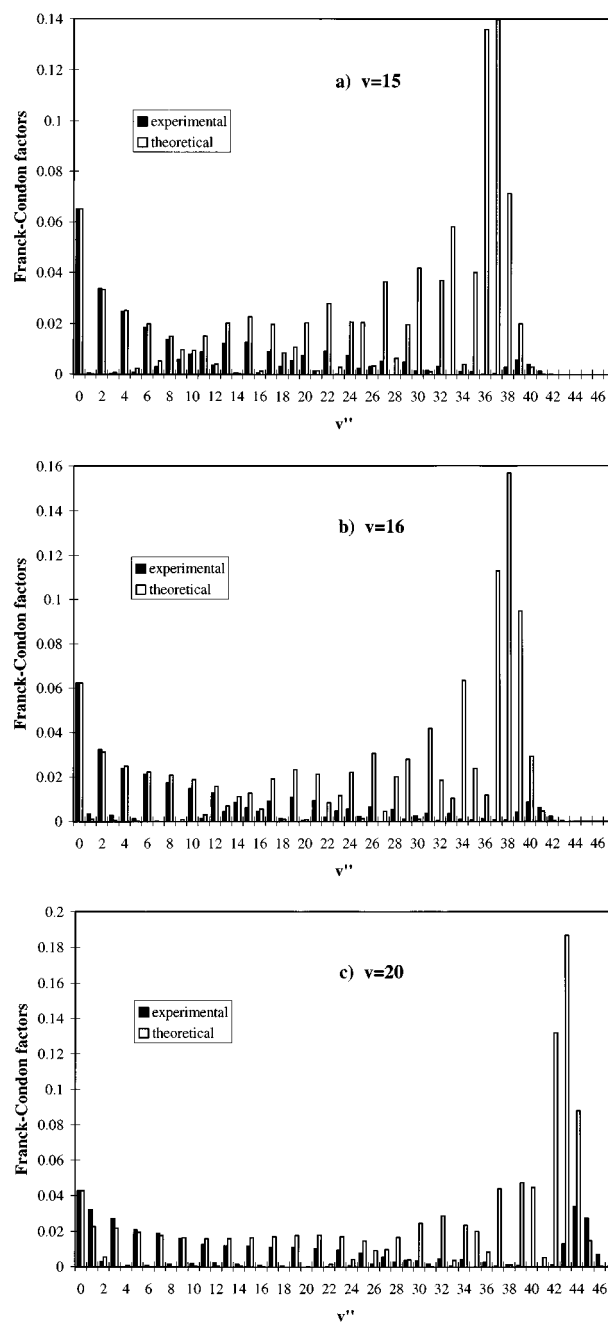
Figure 3 shows the experimental and theoretical FCF's

FIG. 3. Experimental and calculated Franck–Condon factors for transitions from $6\,^1\Sigma^+(v,J=31)$ to different $1(X)^1\Sigma^+(v'',J''=30,32)$ levels. (a) $v = 15$, (b) $v = 16$, (c) $v = 20$. Experimental values are normalized to the theoretical values at $v''=0$.

for the violet emissions from different $6\,^1\Sigma^+(v,J)$ levels. The experimental data are corrected for the variation of the detection system efficiency with wavelength. It can be seen that in each case, the observed pattern of strong and weak lines is reproduced fairly well in the calculations for $v'' \lesssim 25$ only. However, the experimental FCF's regularly become smaller (relative to the calculated values) with increasing vibrational number of the ground state. This decrease in the FCF values most likely results from a decrease in the transition dipole moment with increasing internuclear sepa-
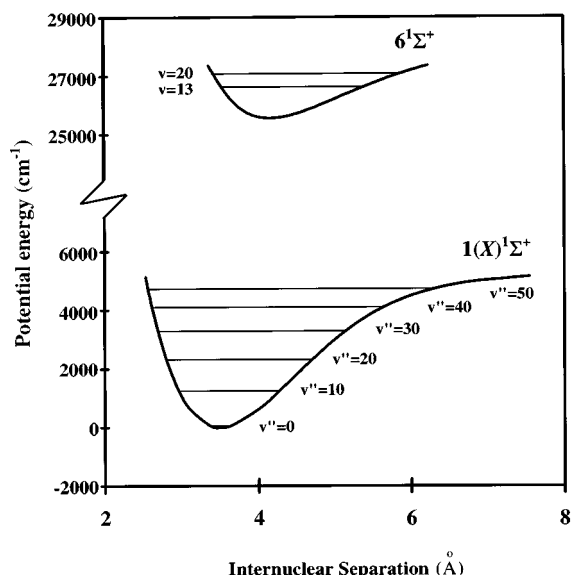
FIG. 4. Experimental RKR potential curves for the $6\,^1\Sigma^+$ state (present work) and $1(X)\,^1\Sigma^+$ state (Ref. 21) as a function of internuclear separation.
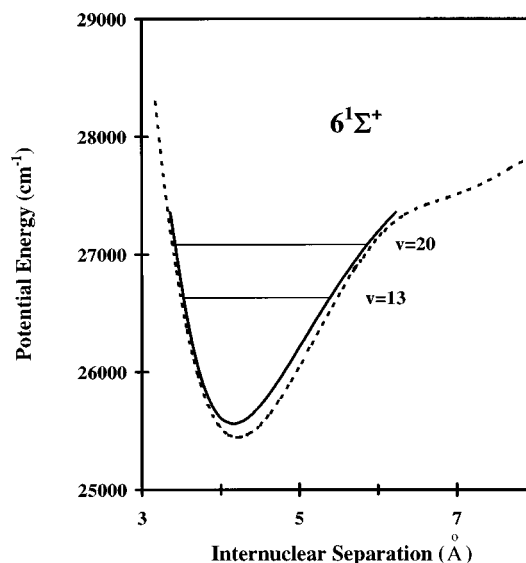

FIG. 5. Comparison of the experimental $6\,^1\Sigma^+$ state RKR potential (solid curve), obtained in the present work, with the theoretical $6\,^1\Sigma^+$ state potential (dashed curve) from Ref. 15.

ration R. However, the locations of the FCF ''zeros'' should be accurately reproduced in the calculation because these are not affected by the variation of the dipole moment. Indeed the experimental intensity zeros are in very good agreement with the calculations for all upper vibrational levels and v'' $\lesssim 25$ (assuming $v_i = 13$). The disagreement for higher v'' must be due to inadequate representation of the $6\,^1\Sigma^+$ state potential well and most likely is the result of the limited

TABLE II. RKR turning points for the NaK $6\,^1\Sigma^+$ state.

ν	R_1 (Å)	R_2 (Å)	$E(\text{cm}^{-1})$
$-1/2$	4.1583	4.1583	0
0	4.0063	4.3305	44.3982
1	3.9061	4.4716	132.1161
2	3.8420	4.5773	218.3726
3	3.7926	4.6688	303.1677
4	3.7516	4.7524	386.5014
5	3.7164	4.8310	468.3737
6	3.6853	4.9061	548.7847
7	3.6574	4.9787	627.7343
8	3.6319	5.0494	705.2225
9	3.6085	5.1189	781.2493
10	3.5868	5.1874	855.8148
11	3.5666	5.2553	928.9188
12	3.5475	5.3227	1000.5615
13	3.5295	5.3900	1070.7428
14	3.5125	5.4571	1139.4627
15	3.4962	5.5244	1206.7212
16	3.4806	5.5919	1272.5183
17	3.4657	5.6598	1336.8541
18	3.4513	5.7281	1399.7285
19	3.4374	5.7971	1461.1415
20	3.4238	5.8667	1521.0931
21	3.4107	5.9371	1579.5833
22	3.3979	6.0084	1636.6122
23	3.3853	6.0808	1692.1797
24	3.3730	6.1542	1746.2857
25	3.3609	6.2289	1798.9304

range of $6\,^1\Sigma^+$ vibrational levels observed in the present work. Figure 4 shows the ground state $1(X)\,^1\Sigma^+$ and the $6\,^1\Sigma^+$ RKR potential curves plotted as a function of internuclear separation, while the turning points of the $6\,^1\Sigma^+$ state RKR potential are listed in Table II. As we can see from Fig. 4, the overlap of the upper and lower state wave functions, for small v'', is dominated by the inner turning point region of the upper state, while the outer turning point region clearly affects the overlap with the ground state wave functions for high v''. In Fig. 5 we show a detailed comparison of the present experimental $6\,^1\Sigma^+$ state RKR potential with the recent theoretical potential of Magnier and Millié.[15] It can be seen that while the general agreement is quite good, the two curves disagree somewhat, especially on the outer limb, and that the theoretical curve shows a ''shelf'' at $R \sim 7$ Å (at even larger internuclear separations, ~ 12 Å, the theoretical calculations predict a second minimum). Such features are due to avoided crossings with other potential curves, but do not affect the present results because they lie above the range of energies probed in this experiment. However, similar interactions could result in small inflections lower down on the outer limb of the true $6\,^1\Sigma^+$ state potential which are not reproduced by the present RKR potential due to the limited data set used in its construction.

D. Collisional line broadening

In the impact limit, which is appropriate for the conditions of the present experiment, the NaK $6\,^1\Sigma^+(v,J)$ $\leftarrow 2(A)\,^1\Sigma^+(v',J') \leftarrow 1(X)\,^1\Sigma^+(v'',J'')$ two-step Doppler-free absorption line shape is a Lorentzian function with full-width-at-half-maximum (FWHM), Γ_{tot}, given by

$$\Gamma_{\text{tot}} = \Gamma_{\text{pred}} + \Gamma_{\text{nat}} + k_{\text{br}}^{\text{Ar}} n_{\text{Ar}} + k_{\text{br}}^{\text{K}} n_{\text{K}} + k_{\text{br}}^{\text{Na}} n_{\text{Na}}. \tag{4}$$

Here Γ_{pred} is the predissociation linewidth, Γ_{nat} is the natural linewidth of the transition, and k_{br}^i represents the broadening

rate coefficient for a particular perturber species with number density n_i. In the present case, collisional line broadening is dominated by collisions with Ar and K atoms, with a minor contribution from Na atom collisions. Specifically, dissociative collisions such as $NaK[6\,^1\Sigma^+(v,J)]+[^{Ar}_K]\rightarrow Na(3S)+K(3D)+[^{Ar}_K]$ and quenching collisions such as $NaK[6\,^1\Sigma^+(v,J)]+K(4S)\rightarrow NaK[1(X)^1\Sigma^+(v'',J'')]+K(3D)$, as well as elastic line broadening collisions, contribute to the overall collision induced linewidth.

For the various $6\,^1\Sigma^+(v,J)\leftarrow 2(A)^1\Sigma^+(v',J')$ transitions investigated in the present work, we obtain the argon broadening rate coefficient k_{br}^{Ar} from the dependence of the measured total linewidth, Γ_{tot}, on the argon gas density at each fixed temperature (fixed alkali atom density). The linewidths are measured by scanning the narrow-band laser over particular $6\,^1\Sigma^+(v,J)\leftarrow 2(A)^1\Sigma^+(v',J')$ transitions, while recording the total atomic and/or molecular emission. The measured total linewidth versus argon density (at fixed temperature) is well represented by a least squares fitted straight line whose slope gives k_{br}^{Ar}. We calculate the broadening rate coefficient as the average of the rates measured at different temperatures for each of a few representative transitions. (We expect that the broadening rate should depend only weakly on temperature; i.e., $k_{br}\propto T^{0.3}$ for van der Waals broadening.[29] Thus, over the temperature range studied here, we expect a variation of k_{br}^{Ar} of less than 5%. This is confirmed by the measured values of k_{br}^{Ar} which generally agree to within that limit.) From data of this type, we obtain $k_{br}^{Ar}=(1.16\pm0.03)$, (1.03 ± 0.05), and $(0.99\pm0.03)\times10^{-8}$ cm^3 s^{-1} for the $6\,^1\Sigma^+(v=14, J=18)\leftarrow 2(A)^1\Sigma^+(v'=16, J'=19)$, $6\,^1\Sigma^+(v=18, J=18)\leftarrow 2(A)^1\Sigma^+(v'=16, J'=19)$, and $6\,^1\Sigma^+(v=20, J=57)\leftarrow 2(A)^1\Sigma^+(v'=16, J'=56)$ transitions, respectively.

We determine the rate coefficients for broadening by alkali perturbers by varying the oven temperature which simultaneously changes both the alkali atomic and molecular densities. Atomic potassium has the highest density at a given temperature, while the density of atomic sodium is about an order of magnitude smaller.[30] The presence of the sodium thus introduces $\sim10\%$ uncertainty into the determination of the potassium broadening rate (assuming that the sodium broadening rate is not too much larger than that due to potassium), since the sodium contribution to the broadening can not be separated out. The molecular (K$_2$, NaK, and Na$_2$) densities are each at least two orders of magnitude smaller than the atomic densities,[30] and their effects can be neglected.

We determine the broadening rate coefficients for atomic potassium perturbers, for the same three transitions as in the study of the broadening by argon, from the slopes of the Γ_{tot} vs potassium density curves. The rate coefficients we obtain from the average slopes of the linear fits for different fixed argon gas pressures are $k_{br}^{K}=(1.4\pm0.5)\times10^{-8}$ cm^3 s^{-1} for the $6\,^1\Sigma^+(v=14, J=18)\leftarrow 2(A)^1\Sigma^+(v'=16, J'=19)$ and $6\,^1\Sigma^+(v=18, J=18)\leftarrow 2(A)^1\Sigma^+(v'=16, J'=19)$ transitions, and $k_{br}^{K}=(5.5\pm2.4)\times10^{-9}$ cm^3 s^{-1} for the $6\,^1\Sigma^+(v=20, J=57)\leftarrow 2(A)^1\Sigma^+(v'=16, J'=56)$ transition. Note that these values have been obtained by multiply-

ing the measured slopes by $n_K/(n_K+n_{Na})$ to partially correct for the broadening effects of atomic sodium. This correction, of $\sim10\%$, is exact if the sodium and potassium broadening rates are equal.

E. Dissociation limit of the repulsive curve

Predissociation is a highly selective process leading directly to product atomic states corresponding to the dissociation limit of the molecular repulsive state inducing the predissociation. In our experiment, we study the predissociation process by monitoring the $K(3\,^2D_{3/2})\rightarrow K(4\,^2P_{1/2})$ atomic fluorescence at 1.17 μm. In order to determine whether $K(3\,^2D_{3/2})$ is the only dissociation product, we also scan the monochromator over the range 1.10–1.30 μm when the two laser frequencies are fixed to pump one of the predissociated states. At the operating temperature of 365 °C and argon pressure of 1.0 Torr, we observe emissions at 1.17, 1.18, 1.24, and 1.25 μm corresponding to the $K(3\,^2D_{3/2})\rightarrow K(4\,^2P_{1/2})$, $K(3\,^2D_{5/2})\rightarrow K(4\,^2P_{3/2})$, $K(5\,^2S_{1/2})\rightarrow K(4\,^2P_{1/2})$, and $K(5\,^2S_{1/2})\rightarrow K(4\,^2P_{3/2})$ transitions, respectively. At this operating temperature and pressure, populations in the $K(3\,^2D_J)$ fine-structure levels are completely mixed by collisions, and there is also significant mixing between $3\,^2D_J$ and $5\,^2S_{1/2}$.

To gain information on the dissociation limit, we reduce the collision rate by lowering the oven temperature and the argon buffer gas pressure. We monitor atomic fluorescence following pumping of the $6\,^1\Sigma^+$ levels $(v=18, J=30)$, $(v=15, J=40)$, $(v=19, J=92)$, and $(v=15, J=94)$ at 257 °C (the lowest temperature at which we are still able to detect atomic fluorescence when pumping most of these levels). In all cases at this low temperature, the 1.24 and 1.25 μm $[K(5\,^2S_{1/2})\rightarrow K(4\,^2P_J)]$ emissions are not observed, while the $K(3\,^2D_{3/2})$ and $K(3\,^2D_{5/2})$ fluorescence signals at 1.17 and 1.18 μm, respectively, are always present with different ratios which are listed in Table III(a). The 1.17 μm/1.18 μm fluorescence ratios $(I_{1.17}/I_{1.18})$ measured for the $6\,^1\Sigma^+(v=18, J=30)$ and $(v=15, J=40)$ levels increase with decreasing argon pressure, while the ratios measured for the $(v=19, J=92)$ and $(v=15, J=94)$ levels are nearly constant (within error bars). This difference in the fluorescence ratio for high J's $(J=92, 94)$ and low J's $(J=30, 40)$ can most likely be attributed to a different predissociation interaction at high J's leading to a different dissociation limit. Atomic fluorescence signals associated with the $(v=15, J=40)$ level could be observed down to $T=217$ °C with no buffer gas. Values of $I_{1.17}/I_{1.18}$ following pumping of this level are listed in Table III(b), where it can be seen that they are roughly constant for different temperatures. We believe that the $6\,^1\Sigma^+(v=15, J=40)$ atomic fluorescence ratios are our most conclusive experimental data for determining the dissociation limit of the $6\,^1\Sigma^+$ predissociation process for lower J levels, since we were able to measure them to lower temperatures and without argon gas.

We base our conclusions on the data taken without any collisional mixing of the two $3\,^2D_J$ fine-structure levels due to argon. However, at the temperatures used $(T$

TABLE III. Ratio of 1.17 to 1.18 μm fluorescence [K($3\,^2D_{3/2} \rightarrow 4\,^2P_{1/2}$)/K($3\,^2D_{5/2} \rightarrow 4\,^2P_{3/2}$)] at (a) different argon buffer gas pressures for different predissociating levels of the NaK $6\,^1\Sigma^+$ state, and (b) at different oven temperatures and no argon gas for the predissociating level $6\,^1\Sigma^+(v=15, J=40)$.

(a)		$I_{1.17}/I_{1.18}$ Argon pressure (Torr)				
$6\,^1\Sigma^+(v,J)$	$T(°C)$	2	1	0.75	0.5	0
(18,30)	257	0.61 ± 0.07	0.67 ± 0.08	0.73 ± 0.09	0.84 ± 0.10	0.93 ± 0.32
(15,40)	256	0.63 ± 0.05				1.49 ± 0.75
(19,92)	255	0.43 ± 0.10	0.48 ± 0.10	0.40 ± 0.12	0.34 ± 0.10	0.43 ± 0.20
						0.50 ± 0.25
(15,94)	257	0.55 ± 0.04	0.63 ± 0.07	0.57 ± 0.10	0.69 ± 0.13	0.64 ± 0.30
						0.75 ± 0.40

(b)		$I_{1.17}/I_{1.18}$ $T(°C)$			
$6\,^1\Sigma^+(v,J)$	256	248	234	227	217
(15,40)	1.49 ± 0.75	1.50 ± 0.75	1.22 ± 0.31	1.40 ± 0.35	1.00 ± 0.40

$=217-256\,°C$), the potassium density[30] ranged from 2.7×10^{14} to 1.2×10^{15} cm^{-3} and thus collisions with ground state potassium atoms can result in significant mixing between the two $3\,^2D_J$ levels. If the two states are completely mixed, the fluorescence ratio $I_{1.17}/I_{1.18}$ should be ~2/3 reflecting the statistical weights of the two levels. If only the $3\,^2D_{5/2}$ level was initially populated, the ratio would be zero in the absence of mixing, and mixing could not increase the ratio to more than 2/3. Since we observe ratios larger than 2/3 (except at high J), we conclude that the $3\,^2D_{3/2}$ fine-structure level must be directly populated by the predissociation process. However, we cannot determine from our data whether the $3\,^2D_{5/2}$ level is populated only by collisions or is also directly populated by predissociation. This question could be answered by studies at lower temperatures where the collisional mixing due to potassium would be negligible. However, we are unable to detect any measurable signals at temperatures below 217 °C. Molecular beam experiments may be required to answer this question definitively.

From the above information, we conclude that the state causing the predissociation (at least for lower J values) must be correlated with either the Na($3\,^2S_{1/2}$)+K($3\,^2D_{3/2}$) atomic state limit only, or with both of the Na($3\,^2S_{1/2}$)+K($3\,^2D_{3/2}$) and Na($3\,^2S_{1/2}$)+K($3\,^2D_{5/2}$) fine-structure limits. Predissociation to the Na($3\,^2S_{1/2}$)+K($3\,^2D_{5/2}$) atomic limit only can be definitely ruled out.

F. Predissociation rates

The predissociation rates can be obtained directly from the measured widths of the $6\,^1\Sigma^+(v,J)\leftarrow2(A)\,^1\Sigma^+(v',J')$ absorption lines. The linewidth is given by Eq. (4). An estimate of the natural linewidth, Γ_{nat} (which is the sum of the radiative decay rates of the upper and lower levels of the transition), is found from studying the dependence of the linewidths of transitions involving nonpredissociating levels on the alkali and argon densities. The various $6\,^1\Sigma^+(v<14,J)$, $6\,^1\Sigma^+(v=14, J<44)$, and $6\,^1\Sigma^+(v=15, J<28)$ levels lie lower than the Na($3S$)+K($3D$) dissociation limit,

and therefore do not predissociate. Thus, for these levels we can set $\Gamma_{pred}=0$ in Eq. (4). We use the values $k_{br}^{Ar}=(1.1\pm0.2)\times10^{-8}$ and $k_{br}^{K}=(1.1\pm0.6)\times10^{-8}$ cm^3 s^{-1} for the argon and potassium line broadening rate coefficients. These are the averages of the values obtained for the various transitions studied (see Sec. III D). The alkali densities are calculated from the Nesmeyanov formulas.[30] For these measurements of the absolute predissociation rates, the experimental conditions were $T=365\,°C$ and $P(Ar)=1.0$ Torr. Once the collisional contributions $k_{br}^{Ar}n_{Ar}+k_{br}^{K}n_{K}+k_{br}^{Na}n_{Na}\sim k_{br}^{Ar}n_{Ar}+k_{br}^{K}[n_k+n_{Na}]$ have been removed from the average linewidth (5.2×10^8 s$^{-1}=83$ MHz of the nonpredissociating levels, we find that the natural radiative rate is given by $\Gamma_{nat}=(1.9\pm0.9)\times10^8$ s^{-1} or $\Delta\nu_{nat}=(30\pm15)$ MHz. Although the radiative rates may vary from level to level, we take this measured value to represent Γ_{nat} for all NaK $6\,^1\Sigma^+(v,J)\leftarrow2(A)\,^1\Sigma^+(v',J')$ transitions.

We measured total linewidths for different transitions involving various $6\,^1\Sigma^+(v,J)$ levels for $v=15, 17, 18, 19$, and 20 and for J's ranging from 9 to 94. Scans showing typical excitation line shapes are displayed in Fig. 6. Total atomic K($3\,^2D_{3/2}\rightarrow4\,^2P_{1/2}$) and molecular NaK[$6\,^1\Sigma^+(v,J)\rightarrow1(X)\,^1\Sigma^+(v'',J\pm1)$] fluorescence signals are monitored as the probe laser is scanned over various NaK $6\,^1\Sigma^+(v,J)\leftarrow2(A)\,^1\Sigma^+(v',J')$ transitions. Two independent indications of predissociation are evident in these signals. First, predissociation results in broadening of the spectral lines (due to shortening of the upper state lifetime) as described by Eq. (4). Second, the shorter lifetime of the strongly predissociating level results in a decrease of molecular (violet band) fluorescence relative to the atomic fluorescence. (In the case of nonpredissociating levels such as $v=14, J=31$, the atomic fluorescence results from collisional processes described in Sec. III D.) It can be seen in the figure that these two indications are consistent. However, the broadening provides a more quantitative measure of the predissociation process. The absolute predissociation rates are obtained by subtracting the natural linewidth and collisional
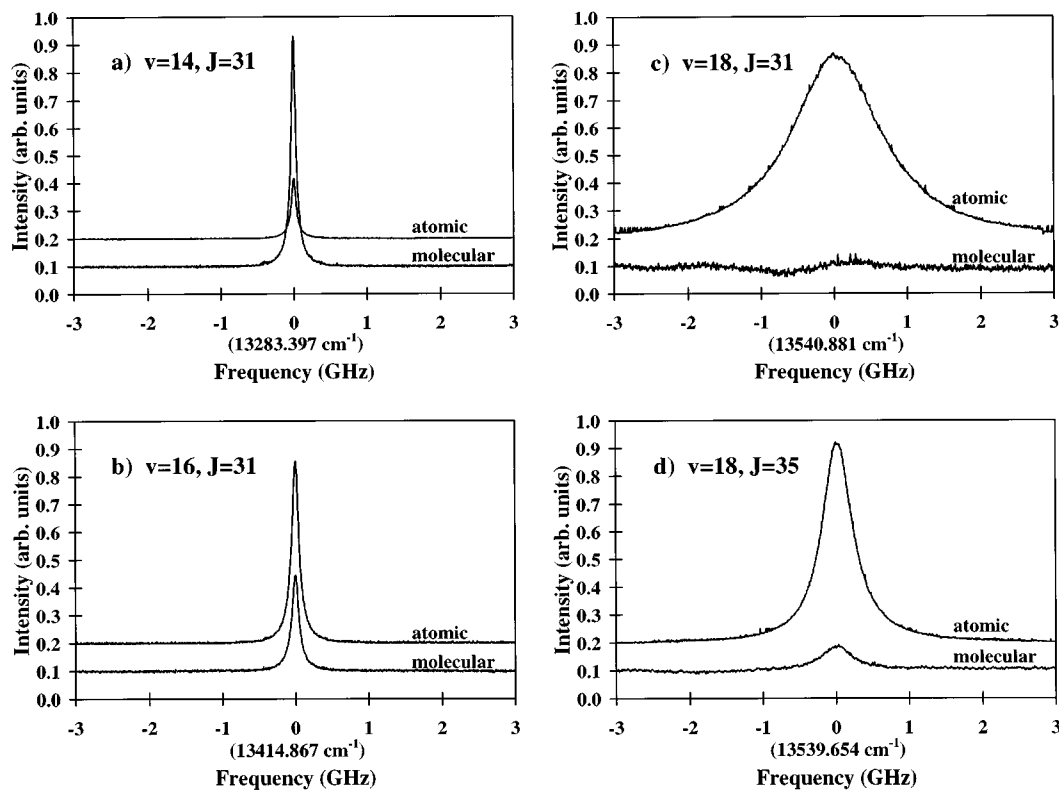
FIG. 6. Probe laser scans over various NaK $6\,^1\Sigma^+(v,J)\leftarrow 2(A)^1\Sigma^+(v',J')$ transitions. In each scan, both the atomic K($3\,^2D_{3/2}\rightarrow 4\,^2P_{1/2}$) and molecular NaK[$6\,^1\Sigma^+(v,J)\rightarrow 1(X)^1\Sigma^+(v'',J\pm 1)$] fluorescence signals are monitored. (a) $v=14$, $J=31$; (b) $v=16$, $J=31$; (c) $v=18$, $J=31$; and (d) $v=18$, $J=35$. The line-center frequency of the transition is given in each panel. In all cases, the fluorescence signals are measured on an arbitrary scale, but the relative atomic/molecular intensity scales are the same for all panels. Note that the strongly predissociating $6\,^1\Sigma^+(v,J)$ levels (i.e., the $v=18$ levels) are characterized by broad lines and large atomic/molecular fluorescence ratios.

rates from the measured linewidths using Eq. (4). The total linewidths were measured with an accuracy of about 20 MHz. However, the uncertainty in the absolute predissociation rates is $\sim$40 MHz due to the correction for the collisional and radiative contributions.

For each of the vibrational levels studied, we plot the absolute predissociation rates as a function of the rotational quantum number J as shown in Fig. 7. A listing of all measured predissociation rates is available in a separate PAPS document.[22] While the strongest predissociations $\Gamma_{pred}\approx 1.6\times 10^9$ to 9.4×10^9 s^{-1} occur for $v=18$ and show a strong resonance behavior centered on $J=29$, the data for some other v levels show an oscillatory J dependence that suggests a variation in the bound and free state vibrational overlap integral. Although the rates for these levels are relatively small (ranging from 0 to $\sim 8\times 10^8$ s^{-1}), it is clear that there is some oscillatory behavior with increasing J for J's $<$70, followed by a general increase in the rates with increasing J at higher values.

G. Predissociation interaction type

Figure 8 shows the six molecular potentials which dissociate to the Na($3S$)+K($3D$) asymptote (according to the calculations of Magnier and Millié[15]) along with the $6\,^1\Sigma^+$ state potential obtained in the present work. It can be seen that $6\,^1\Sigma^+$ is crossed by the $5\,^3\Sigma^+$ state on its right limb,

and by the $3\,^1\Pi$ state on both limbs. The calculations of Stevens et al.[14] also show crossings of the $6\,^1\Sigma^+$ state potential with the $5\,^3\Sigma^+$ and $3\,^1\Pi$ states on the right limb, as well as a crossing with the $3\,^3\Pi$ state on the right limb. (The Magnier calculations show an avoided crossing of the $3\,^3\Pi$ and $4\,^3\Pi$ states forcing the former to have a double minimum.) Figure 9 presents a correlation diagram showing how the Hund's case (a) or (b) molecular states at small internuclear separation first transform into Hund's case (c) states and then into the Na($3\,^2S_{1/2}$)+K($3\,^2D_J$) separated atom limits with increasing separation. The small R limits are based on the ordering of Magnier and Millié[15] (which is identical to that of Stevens et al.[14]) at $R=8\ a_0$ (4.23 Å). Note that the potassium $3\,^2D_J$ levels are inverted.[20] From this diagram, we find that all three states ($5\,^3\Sigma^+$, $3\,^1\Pi$, and $3\,^3\Pi$) correlate with the Na($3\,^2S_{1/2}$)+K($3\,^2D_{3/2}$) limit.

The rates of predissociation are directly related to the type of perturbative interaction causing the predissociation, and to the overlap of the vibrational wave functions of the bound and free states. In general, $\Gamma_{pred}=2\pi|H_{v,J;E,J}|^2$, where $H_{v,J;E,J}$ is the matrix element of the interaction causing the predissociation which couples the bound state v, J to the continuum state represented by E, J.[31] If the matrix element of the interaction is assumed to be independent of R or to vary linearly with R, then it can be factored as $\Gamma_{pred}=2\pi(H_{el})^2|\langle\psi_{v,J}(R)|\psi_{E,J}(R)\rangle|^2$, where H_{el} is the constant
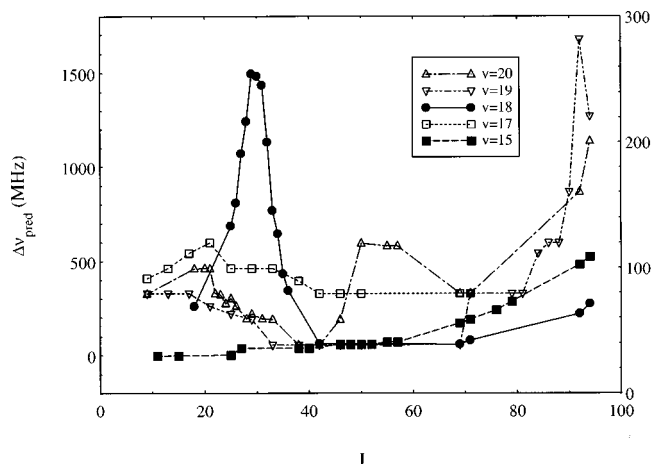
FIG. 7. Absolute predissociation rates vs J for different vibrational levels. The data for $v=15$ and $v=18$ correspond to the vertical scale on the left, while those for $v=17$, 19, and 20 correspond to the vertical scale on the right.

FIG. 9. Correlation diagram for the NaK molecule at the Na($3\,^2S$) + K($3\,^2D$) dissociation limit. The diagram shows the transition from the Hund's case (a) or (b) molecular states on the left (the ordering is that given by the theoretical potentials of Ref. 15 at $R=8\;a_0$) into the Hund's case (c) states, and finally into the separated atom limits on the right. Note that the potassium $3\,^2D_J$ levels are inverted (Ref. 20).

electronic factor (if the interaction is independent of R) or the electronic factor evaluated at the R-centroid value (if the interaction varies linearly with R). Here, $|\langle\psi_{v,J}(R)|\psi_{E,J}(R)\rangle|^2$ is the differential Franck–Condon factor, assuming that the continuum state wave function $\psi_{E,J}(R)$ is energy normalized. If the interaction is J dependent (i.e., for $\Delta\Omega\neq0$ interactions), then a similar analysis yields $\Gamma_{\mathrm{pred}}=2\pi(H_{\mathrm{el}})^2|\langle\psi_{v,J}(R)|\hbar^2/2\mu R^2|\psi_{E,J}(R)\rangle|^2$ $\times\;[J(J+1)-\Omega(\Omega+1)]\cong\;2\pi(H_{\mathrm{el}})^2(\hbar^2/2\mu R_c^2)^2$ $\times|\langle\psi_{v,J}(R)|\psi_{E,J}(R)\rangle|^2[J(J+1)-\Omega(\Omega+1)]$, where R_c is the internuclear separation of the crossing between the bound and continuum states.[31]

If the interaction H_{el} between the bound and unbound states is independent of J, the dependence of the predissociation rate on J directly reflects the dependence of the radial wave function overlap integral on J. This in turn, is a func-
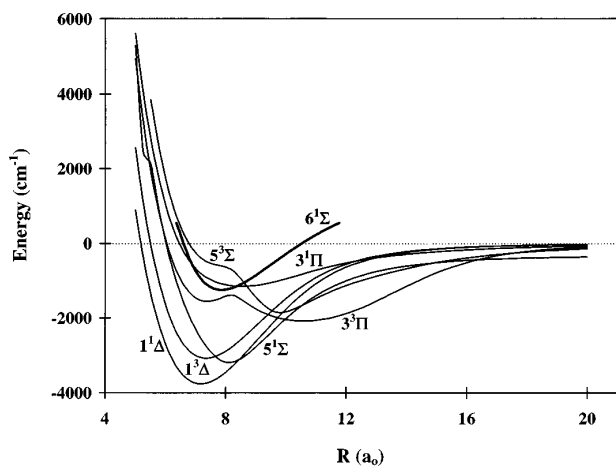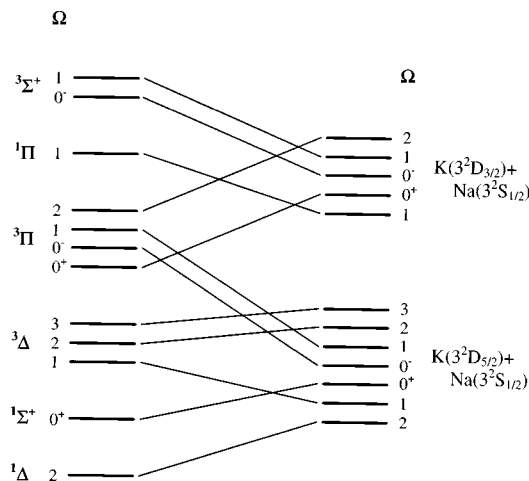

FIG. 8. NaK states near the Na($3\,^2S$) + K($3\,^2D$) separated atom limit. The thin solid curves are the Magnier and Millié (Ref. 15) theoretical potentials correlating at large separation to the Na($3\,^2S$) + K($3\,^2D$) asymptote. The thick solid curve is the $6\,^1\Sigma^+$ potential [correlating to the Na($3\,^2S$) + K($5\,^2P$) asymptote], determined experimentally in the present work. The zero of energy is taken to be the Na($3\,^2S$) + K($3\,^2D$) separated atom limit.

tion of the curve crossing scheme. Mulliken has classified the various curve crossing schemes according to the labels a, b, and c, which indicate whether the energy of the crossing point is equal to, below, or above the dissociation energy of the continuum state causing the predissociation.[32] In addition, the superscripts $-$, i, and $+$, are used to indicate whether R_c is less than, equal to, or greater than the equilibrium separation of the bound state, or 0 is used to indicate that the states do not cross.[32] Depending on the crossing scheme and on the steepness of the curves, the two wave functions will come into and out of phase as we move from one vibrational level to another, or from one rotational level to another. In this case, the maximum predissociation rate occurs when the overlap is a maximum, and this usually occurs for bound state levels with energies near the curve crossing point. In the present case, the largest predissociation rates are observed for $v=18$, and from this observation we might conclude that the bound and free state curve crossing must occur near $v=18$ of the $6\,^1\Sigma^+$ state. If this hypothesis is correct, the dependence of the predissociation rates on v and J could, in principle, be predicted by assuming a particular picture of the curve crossing and calculating the overlap integrals between the corresponding bound and free state wave functions. The shape of the free state could then be varied until good agreement is achieved between the observed and calculated v and J dependences of the predissociation rates.[31,33] However, based on the theoretical potentials of Ref. 15 (see Fig. 8) it appears likely that the crossing points of $6\,^1\Sigma^+$ with the $5\,^3\Sigma^+$ and $3\,^1\Pi$ states occur below the Na($3\,^2S$) + K($3\,^2D$) asymptote (Mulliken's type b$^+$ crossing), and thus well below the turning point of $6\,^1\Sigma^+$($v=18$). Predissociation of $6\,^1\Sigma^+$ by $3\,^3\Pi$ would be classified as type b^0 predissociation, since these two states do not cross at all according to the theoretical curves. Moreover, due to the sensitivity of the overlap integrals to the wave

functions, in order to obtain any reliable results from the calculations, the bound state must be known with better accuracy than we now possess (especially near the outer turning point).

The selection rules for predissociation are $\Delta J = 0$, $+ \leftrightarrow -$, and in addition $\Delta \Lambda = 0$, ± 1, and $\Delta S = 0$, ± 1 in Hund's case (a) or (b), and $\Delta \Omega = 0$, ± 1 in Hund's case (c). The $3\,^3\Pi$ state correlates to both $\mathrm{Na}(3\,^2S_{1/2}) + \mathrm{K}(3\,^2D_{3/2})$ and $\mathrm{Na}(3\,^2S_{1/2}) + \mathrm{K}(3\,^2D_{5/2})$ atomic limits, and can cause predissociation of the $6\,^1\Sigma^+$ state through spin–orbit interactions {specifically the $^3\Pi_{0+}$ component [which correlates to the $\mathrm{Na}(3\,^2S_{1/2}) + \mathrm{K}(3\,^2D_{3/2})$ limit] interacts with $6\,^1\Sigma^+$}. The $3\,^1\Pi$ and $5\,^3\Sigma^+$ states correlate only to the $\mathrm{Na}(3\,^2S_{1/2}) + \mathrm{K}(3\,^2D_{3/2})$ atomic limit, and can interact with $6\,^1\Sigma^+$ through the L-uncoupling operator (gyroscopic perturbations), which increase with J. However, nonadiabatic mixing between states of the same symmetry can result in some dissociation to the $\mathrm{Na}(3\,^2S_{1/2}) + \mathrm{K}(3\,^2D_{5/2})$ limit. Although it is difficult to pinpoint the exact nature of the $6\,^1\Sigma^+$ state predissociation, we believe the $3\,^1\Pi$ or $5\,^3\Sigma^+$ state is most likely responsible for the predissociation observed at high J while $3\,^3\Pi$ is probably responsible for the predissociation observed at intermediate J.

While the argument of a curve crossing on the outer limb of $6\,^1\Sigma^+$ might be adequate to interpret our intermediate J data, it does not explain the fact that the largest predissociation rates for $v = 18$ are three to ten times larger than the peak rates measured for the other vibrational levels. This implies that the predissociation of $v = 18$ might be caused by a different interaction than that causing the predissociation of the other vibrational levels. Therefore, it is possible that the resonance behavior at $v = 18$ is not due to a curve crossing at that point, but rather to an accidental predissociation, where the initial $6\,^1\Sigma^+$ state is perturbed by another state, and this second state in turn undergoes predissociation by yet another state. An accidental predissociation is difficult to characterize because it involves two perturbative interactions and three potential curves. For accidental predissociation, the $6\,^1\Sigma^+$ state must be perturbed by another state with an interaction which satisfies the perturbation selection rules. The state causing the perturbation is then perturbed by the continuum of a third state that causes the former to predissociate. Here, the predissociation selection rules (which are the same as the selection rules for perturbations) must again be satisfied. An attractive possibility is that the $6\,^1\Sigma^+$ state interacts with the $4\,^3\Pi$ state via spin–orbit interactions, and the latter state is predissociated by nonadiabatic interactions with the $3\,^3\Pi$ state. However, further speculation should be left until additional experimental and theoretical work provides a more accurate mapping of the NaK potentials in this energy region.

Homogeneous interactions ($\Delta \Omega = 0$) are independent of J (Ref. 31) and therefore cannot explain the observed increase of predissociation rates with J at high J (see Fig. 7). However, heterogeneous (J-dependent) gyroscopic predissociations exhibit a quadratic dependence on J. Gyroscopic predissociation of the $6\,^1\Sigma^+$ state by $3\,^1\Pi$ or $5\,^3\Sigma^+$ is possible according to the selection rules for heterogeneous pre-

dissociation [$\Delta S = 0$ (weak selection rule) and $\Delta \Omega = \pm 1$]. The predissociation rates for $v = 15$ show a consistent increase with the rotational quantum number J, without showing any oscillations. The nearly quadratic dependence of the rates on J for $v = 15$ implies that the interaction might be due to gyroscopic predissociation. This interpretation is consistent with our measured values of $I_{1.17}/I_{1.18}$ (see Sec. III E), which led us to conclude that the predissociation mechanism was different at high and low J.

H. Collisional processes involving excitation transfer between rotational levels of the NaK $2(A)^1\Sigma^+$ state

1. J-changing collisions

We have observed collisional excitation transfer between different rotational levels of the $2(A)^1\Sigma^+$ state,

$$\mathrm{NaK}(v,J) + P \xrightarrow{k^P_{J \to J'}} \mathrm{NaK}(v,J') + P, \tag{5}$$
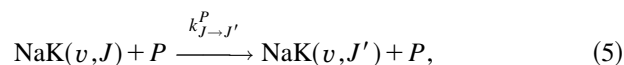
where P represents the perturber which can be any of the species present in the vapor (Ar, K, Na, K_2, NaK, Na_2) and $k^P_{J \to J'}$, is the rate coefficient for the process. This phenomenon results in the appearance of satellite lines (see Fig. 10) that are observed when the frequency of the Ti–sapphire laser is scanned in the vicinity of a specific $6\,^1\Sigma^+(v,J) \leftarrow 2(A)^1\Sigma^+(v',J')$ transition, after the $2(A)^1\Sigma^+(v',J')$ level has been prepared by pumping with a separate laser on a particular transition from the ground $1(X)^1\Sigma^+$ state. These satellite lines correspond to transitions involving nearby J' levels of the A state that are populated through collisions; i.e., $6\,^1\Sigma^+(v,J \pm 1, J \pm 2, \ldots) \leftarrow 2(A)^1\Sigma^+(v',J' \pm 1, J' \pm 2, \ldots)$.

An approximate rate coefficient for this process can be determined from the relative intensities of the main peak and the satellite lines, combined with a simple rate equation model. The change in density of atoms in the collisionally populated rotational levels can be represented by rate equations of the following form:

$$\frac{dn_{J' \pm n}}{dt} = R_{J' \to J' \pm n} n_{J'} - \Gamma_{J' \pm n} n_{J' \pm n}. \tag{6}$$

Here, $R_{J' \to J' \pm n}$ is the rate of population transfer from the J' to $J' \pm n$ level and $\Gamma_{J' \pm n}$ is the radiative decay rate out of the $J' \pm n$ level. Back transfer from level $J' \pm n$ to level J' can be neglected. In steady state, Eq. (6) yields the ratio of the populations in the $J' \pm n$ and J' levels, $(n_{J' \pm n}/n_{J'}) = (R_{J' \to J' \pm n}/\Gamma_{J' \pm n})$. The ratio of the satellite to main line intensities, shown in Fig. 10(a), is approximately proportional to this ratio. From the data of Figs. 10(a) and 10(b), we obtain the intensity ratio (0.041 ± 0.010) for the $\Delta J' = +1$ excitation transfer collision, which yields $R_{J' \to J'+1} = (0.041)\Gamma_{J'+1}$. An absolute value of $R_{J' \to J'+1}$ could be obtained if the radiative rate $\Gamma_{J'+1}$ was known. Since $\Gamma_{J'+1}$ is on the order of 2×10^8 s^{-1} (corresponding to a 5 ns lifetime), we obtain an approximate value $R_{J' \to J'+1} \approx 8.2 \times 10^6$ s^{-1}. The J-changing collision rate coefficient
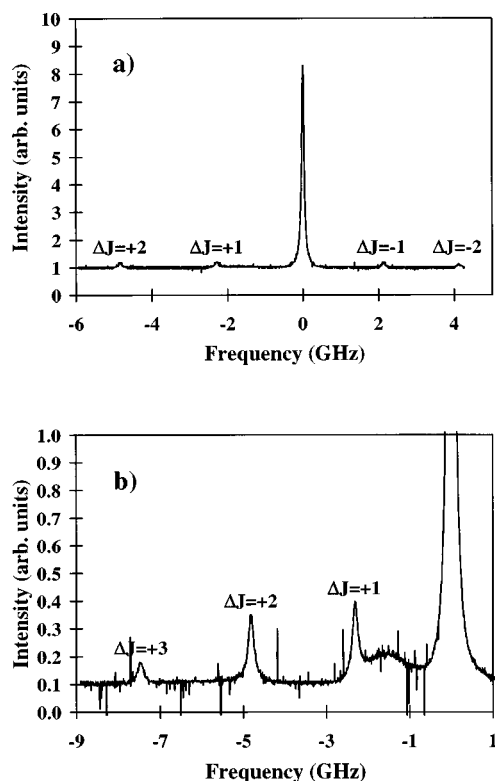
FIG. 10. (a) Ti–sapphire laser frequency scan showing the main line corresponding to the $6\,^1\Sigma^+(v=13, J=31)\leftarrow2(A)\,^1\Sigma^+(v=16, J=30)$ transition ($13\,215.798$ cm^{-1} line-center frequency, ~80 MHz linewidth), and the satellite peaks labeled $\Delta J=+2$, $\Delta J=+1$, $\Delta J=-1$, and $\Delta J=-2$ [identified as $6\,^1\Sigma^+(v=13, J=33)\leftarrow2(A)\,^1\Sigma^+(v=16, J=32)$, $6\,^1\Sigma^+(v=13, J=32)\leftarrow2(A)\,^1\Sigma^+(v=16, J=31)$, $6\,^1\Sigma^+(v=13, J=30)\leftarrow2(A)\,^1\Sigma^+(v=16, J=29)$, and $6\,^1\Sigma^+(v=13, J=29)\leftarrow2(A)\,^1\Sigma^+(v=16, J=28)$]. (b) Sensitivity increased by a factor of 10 clearly showing the relative amplitudes of the satellite lines and their linewidths (~180 MHz). The broad feature between the main peak and the $\Delta J=+1$ peak in (b) is an unidentified Doppler-broadened transition from the ground state involving two probe laser photons (rather than one pump and one probe photon used in the two-step transitions).

$k^P_{J'\rightarrow J'+1}$ can then be calculated from $R_{J'\rightarrow J'+1}$ and the perturber number density ($n_p\sim2.6\times10^{16}$ cm^{-3} at $T=365\,°C$),

$$k^P_{J'\rightarrow J'+1}=\frac{R_{J'\rightarrow J'+1}}{n_p}\approx3.1\times10^{-10}\ \text{cm}^3\ \text{s}^{-1}\pm50\%,$$
(7a)

Similarly, we obtain

$$k^P_{J'\rightarrow J'+2}=\frac{R_{J'\rightarrow J'+2}}{n_p}\approx2.6\times10^{-10}\ \text{cm}^3\ \text{s}^{-1}\pm50\%$$
(7b)

and

$$k^P_{J'\rightarrow J'+3}=\frac{R_{J'\rightarrow J'+3}}{n_p}\approx0.84\times10^{-10}\ \text{cm}^3\ \text{s}^{-1}\pm50\%$$
(7c)

for collisional transitions of $+2$ and $+3$ rotational units, respectively. These data were taken under conditions where the oven was operated in the heat-pipe mode. Thus we assume that the majority of the perturbers are potassium atoms in this case. The major sources of error in these rate coefficients are uncertainties in $\Gamma_{J'\pm n}$ and in the potassium density. Note that the above results on rotational energy transfer are based upon collisional transitions involving only one initial level; $2(A)\,^1\Sigma^+(v'=16, J'=30)$. Clearly a more comprehensive study is desirable.

2. Velocity-changing collisions

A careful inspection of the widths of the lines resulting from the excitation transfer between different rotational levels discussed above shows that the lines originating from a collisionally populated level are broader than those directly pumped by the laser. Figure 10(a) shows a probe laser frequency scan over a few of these lines, while Fig. 10(b) shows the same lines on a much more sensitive scale where the linewidths can be measured. It is clear from analysis of this figure that the collisionally populated levels give rise to spectral lines which are ~100 MHz broader than the main line.

We attribute this broadening effect to velocity-changing collisions. The narrow bandwidth of the ring dye laser used to pump the A state level results in excitation of a single velocity class. When molecules in the level (v', J') undergo state-changing collisions, they simultaneously experience velocity changes which tend to thermalize their velocity distribution. If the collision rate was much larger than the radiative rate, the excited molecules would undergo a series of these velocity-changing collisions. Under such conditions, the velocity distribution would become completely thermalized and the velocity spread would then reflect a Maxwell–Boltzmann distribution. In the present case, only one or two collisions occur within a radiative lifetime, and thus the thermalization is far from complete. The details of the thermalization process depend on the type of interaction between the NaK molecule in a particular J' level of the A state, and the perturbing species causing the state- and velocity-changing process. In order to draw any conclusions about the type of interaction causing the velocity-changing collision process, further investigations are needed, and this will be the topic of a future experiment planned in our lab. The dependence of the line shape on the argon and alkali metal densities can provide information on the dominant perturbing species, the thermalization process, and the NaK–Ar and NaK–alkali interaction potentials. These potentials are not currently available, either from experiment or theory.

IV. CONCLUSIONS

We have carried out two-step excitation of the $6\,^1\Sigma^+$ state of NaK in order to study the bound–bound $6\,^1\Sigma^+\rightarrow1(X)\,^1\Sigma^+$ molecular fluorescence and predissociation of the $6\,^1\Sigma^+$ state to the $\text{Na}(3\,^2S_{1/2})+\text{K}(3\,^2D_J)$ separated atom limit. From analysis of the $6\,^1\Sigma^+\leftarrow2(A)\,^1\Sigma^+$ excitation spectra and experimental $6\,^1\Sigma^+\rightarrow1(X)\,^1\Sigma^+$ band Franck–Condon factors, we obtained molecular constants describing the $6\,^1\Sigma^+$ state.

Widths of individual $6 {}^1\Sigma^+(v,J'\pm1)$ $\leftarrow 2(A){}^1\Sigma^+(v',J')$ excitation lines are determined by collisional broadening and the lifetimes of the levels. The latter depend upon the natural radiative rates and the $6 {}^1\Sigma^+(v,J'\pm1)$ level predissociation rates. We measured broadening rates for several $6 {}^1\Sigma^+(v,J'\pm1)\leftarrow 2(A){}^1\Sigma^+(v',J')$ transitions due to collisions with argon and potassium perturbers. By correcting the total linewidth for collisional and natural broadening we have mapped the $6 {}^1\Sigma^+$ state predissociation rates on a level by level basis for v ranging from 15 to 20 and J values in the range 9–94. We have also observed state-changing and velocity-changing collisions of NaK molecules in the $2(A){}^1\Sigma^+(v'=16, J'=30)$ level interacting with potassium and argon perturbers.

ACKNOWLEDGMENTS

[1] K. H. Meiwes and F. Engelke, Chem. Phys. Lett. **85**, 409 (1982).

[2] E. J. Breford and F. Engelke, Chem. Phys. Lett. **75**, 132 (1980).

[3] C. Brechignac and Ph. Cahuzac, Chem. Phys. Lett. **112**, 20 (1984).

[4] J. Heinze, P. Kowalczyk, and F. Engelke, J. Chem. Phys. **89**, 3428 (1988).

[5] H. Katô, T. Kobayashi, M. Chosa, T. Nakahori, T. Lida, S. Kasahara, and M. Baba, J. Chem. Phys. **94**, 2600 (1991).

[6] H. Katô, T. Kobayashi, Y. C. Wang, and K. Ishikawa. Chem. Phys. **162**, 107 (1992).

[7] H. Katô, T. Kumauchi, K. Nishizawa, and M. Baba, J. Chem. Phys. **98**, 6684 (1993).

[8] S. F. Rice, X. Xie, and R. W. Field, Chem. Phys. **104**, 161 (1986).

[9] I. Schmidt, W. Meyer, B. Krüger, and F. Engelke, Chem. Phys. Lett. **143**, 353 (1988).

[10] H. Katô and K. Onomichi, J. Chem. Phys. **82**, 1642 (1985).

[11] S. Kasahara, M. Baba, and H. Katô, J. Chem. Phys. **94**, 7713 (1991).

[12] H. Ikoma, S. Kasahara, and H. Katô, Mol. Phys. **85**, 799 (1995).

[13] B. K. Clark, M. Masters, and J. Huennekens, Appl. Phys. B **47**, 159 (1988).

[14] W. J. Stevens, D. D. Konowalow, and L. B. Ratcliff, J. Chem. Phys. **80**, 1215 (1984).

[15] S. Magnier and Ph. Millié, Phys. Rev. A **54**, 204 (1996).

[16] S. Kasahara, H. Ikoma, and H. Katô, J. Chem. Phys. **100**, 63 (1994).

[17] L.-E. Berg, M. Beutter, and T. Hansson, Chem. Phys. Lett. **253**, 327 (1996).

[18] T. Hansson (unpublished results).

[19] G. Herzberg, *Molecular Spectra and Molecular Structure I. Spectra of Diatomic Molecules* (Krieger, Malabar, 1989).

[20] C. E. Moore, *Atomic Energy Levels*, National Bureau of Standards Circular 467 (U.S. Government Printing Office, Washington, D.C., 1949), Vol. 1.

[21] A. J. Ross, C. Effantin, J. d'Incan, and R. F. Barrow, Mol. Phys. **56**, 903 (1985).

[22] See AIP document No. PAPS JCPSA-107-1094-5 for 5 pages of tables. Order by PAPS number and journal reference from American Institute of Physics, Physics Auxiliary Publication Service, Carolyn Gehlbach, 500 Sunnyside Bouldevard, Woodbury, NY 11797-2999. Fax: 516-576-2223, e-mail: paps@aip.org. The price is $1.50 for each microfiche (98 pages) or $5.00 for photocopies of up to 30 pages, and $0.15 for each additional page over 30 pages. Airmail additional. Make checks payable to the American Institute of Physics.

[23] R. Rydberg, Z. Phys. **73**, 376 (1931).

[24] O. Klein, Z. Phys. **76**, 226 (1932).

[25] A. L. Rees, Proc. Phys. Soc. London A **59**, 998 (1947).

[26] R. J. LeRoy, RKR1: A computer program implementing the first-order RKR method for determining diatom potential energy curves from spectroscopic constants, University of Waterloo, Chemical Physics Research Report No. CP-425, 1992.

[27] R. J. LeRoy, LEVEL 6.0: A computer program solving the radial Schrödinger equation for bound and quasibound levels, and calculating various expectation values and matrix elements, University of Waterloo, Chemical Physics Research Report No. CP-555, 1995.

[28] P. F. Bernath, *Spectra of Atoms and Molecules* (Oxford University Press, New York, 1995).

[29] A. Corney, *Atomic and Laser Spectroscopy* (Clarendon, Oxford, 1977).

[30] A. N. Nesmeyanov, *Vapor Pressure of the Elements* (Academic, New York, 1964).

[31] H. Lefebvre-Brion and R. W. Field, *Perturbations in the Spectra of Diatomic Molecules* (Academic, Orlando, 1986).

[32] R. S. Mulliken, J. Chem. Phys. **33**. 247 (1960).

[33] M. S. Child, in *Molecular Spectroscopy*, edited by R. F. Barrow, D. A. Long, and D. J. Millen (Chemical Society, London, 1974), Vol. 2, p. 466.